Spar I Liquid Mixing Experiment

C. F. Schafer* and G. H. Fichtl†
NASA Marshall Space Flight Center, Huntsville, Ala.

The first Space Processing Applications Rocket (SPAR I) payload flew in December 1975. The liquid mixing experiment had as its objective the observation of effects of residual acceleration of this payload on a confined fluid system. The fluid system was chosen to be similar geometrically and in fluid properties to a range of materials science experiments. Samples were constructed as cylinders 2.2 cm long by 0.6 cm diameter. Half (1.1 cm) of each cylinder was composed of pure indium, and the other half of each was an alloy of 80 wt% indium and 20 wt% lead. The samples were enclosed in aluminum cartridges and placed in heaters mounted in three mutually perpendicular directions. The experimental procedure consisted of melting the samples when the low-g phase of the payload trajectory was attained, holding the samples in a molten state for approximately 200 seconds, and then quenching to resolidification before leaving low g. The returned samples were analyzed by x-ray radiography to determine the nature of the flows experienced. Two of the samples exhibited very little fluid motion. The third sample, which was oriented nearly parallel to a payload radius, showed a great deal of flow. These observations were shown to be consistent with the action of a constant body force in the 10^{-6} g to 10^{-5} g range.

I. Introduction

PART of the motivation for performing materials science experiments in space has been that convective mass transport and heat transfer in fluids containing density gradients could be suppressed by removal of the gravitational body force. These convective flows were known to influence the quality of certain solid products formed from a fluid state. A number of materials science experiments have been performed in the low-gravity environments of Skylab and Apollo-Soyuz which demonstrated improvements in some material properties, those improvements being related to a quiescent fluid state.[1,2] In addition, a few phenomenological experiments and science demonstrations directly related to fluid physics have been flown. Examples of these are the Benard convection experiment on Apollo 14[3] and the Skylab science demonstrations.[4] One important conclusion from these studies is that in a low-gravity environment, surface tension can become a dominant influence in both fluid statics and dynamics. The Skylab radioactive tracer experiment, M558, could be considered a fluid mechanics experiment as well.[5] Results from that experiment demonstrated that for the experimental configuration used, convective flow made no appreciable contribution to the measured mass transfer. Materials science related fluid experiments then, through Apollo-Soyuz, did little to link residual spacecraft accelerations to fluid motions.

The Space Processing Applications Rocket (SPAR) program offered materials science experimentors a platform for performing a large number of low-g experiments in the interim period between Apollo-Soyuz and Spacelab. The experiment described here flew on the first SPAR payload in Dec. 1975. Its objective was to observe the effects of the sounding rocket accelerative environment on a confined fluid system (containing density gradients), which is a relevant model for other space processing experiments. Results from this experiment should serve several purposes. First, they should aid in characterizing the rocket environment. Second, they should emphasize the importance of planning low-g experiments carefully with respect to possible motions even at very low acceleration levels. Third, they should furnish further data for evaluating the usefulness of computations for semiquantitative predictions of fluid behavior in this and similar configurations.

Presented as Paper 77-119 at the AIAA 15th Aerospace Sciences Meeting, Los Angeles, Calif., Jan. 24-26, 1977; submitted Feb. 1, 1977; revision received Feb. 13, 1978.

Index categories: Subsonic Flow; Sounding Rocket Systems.

*Physicist, Space Sciences Laboratory.
†Fluid Dynamicist, Space Sciences Laboratory. Member AIAA.

II. Experiment Design

This experiment aims at observing the effects of coupling of gravitational-type body forces with density gradients in the liquid sample. In order to isolate this type of effect, other factors tending to drive fluid motion had to be minimized. Several possible extraneous effects were considered in the experiment design. These are summarized in Table 1. The effects listed here were minimized by a system selection and sample container design.

In addition, sample size, shape, and composition were chosen to be representative of a range of space processing experiments. Samples were cylinders 2.2-cm long and 0.6-cm in diameter. One half (1.1 cm) of each sample was composed of 5N pure indium, while the other end (1.1 cm) was composed of an alloy of 20-wt% lead and 80-wt% indium (Fig. 2). The samples were assembled and placed in aluminum cartridges containing expansion volumes at each end. The cartridges were mounted in three mutually perpendicular orientations in a Thermal Control Unit (TCU) (Fig. 3), and the complete experiment configuration was mounted in the Black Brant payload section as shown in Fig. 4. The TCU

Table 1 Extraneous variables in experiment

Effect	Comments
Buoyancy convection due to temperature gradients	Temperature gradients too low for this effect
Thermocapillary convection	Temperature gradients too low for this effect
Solutocapillary convection	No concentration gradients present at the liquid-gas interface
Volume change with phase change	This should lead to uniform expansion and contraction of the sample, but not to distortion. Materials selected for small volume change at phase change
Nonuniform melting of sample	Materials chosen so that melting points are very close together (phase diagram shown in Fig. 1)

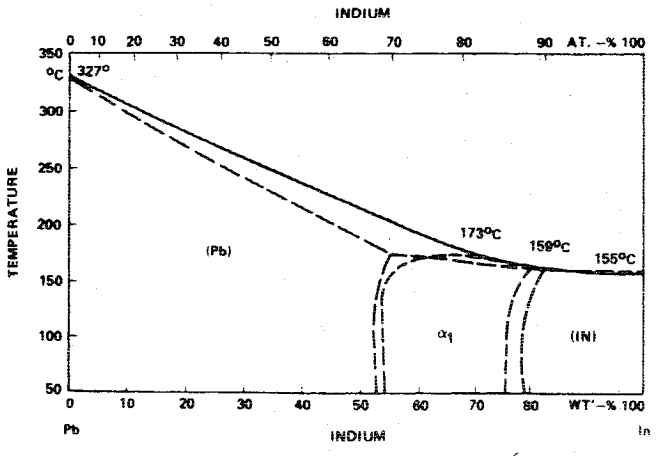

Fig. 1 In-Pb phase diagram (from Hansen[6]).

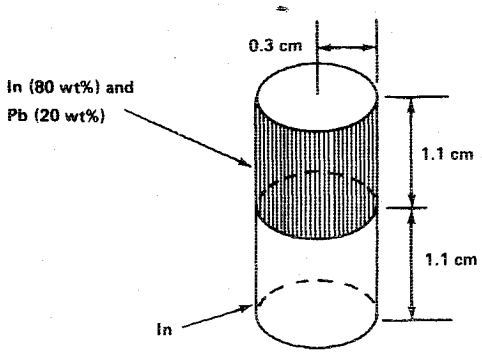

Fig. 2 Sample configuration.

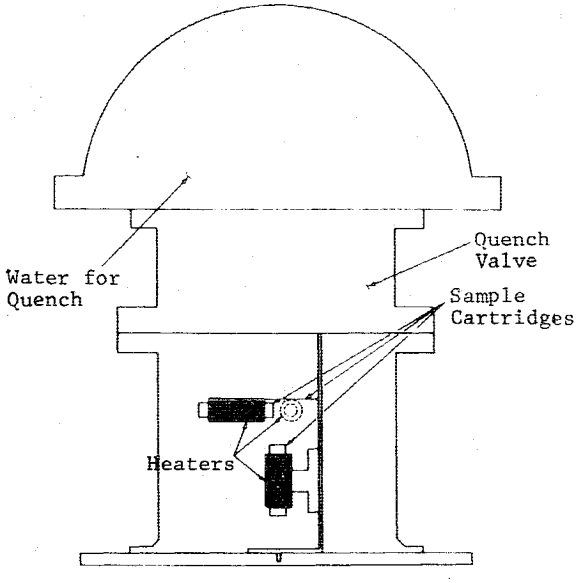

Fig. 3 Thermal control unit.

provided heaters, temperature sensing, and water quench for the samples, these functions being controlled by a timing circuit activated at launch. Through ground-based testing, a time line was established for conducting the experiment within the low-g portion of the payload trajectory. Sample heating was initiated at launch plus 45 s. Heaters were turned off at launch plus 225 s, and quench occurred at launch plus 345 s. This schedule allowed some margin of error in the estimate that low g (10^{-4} g or less) would be encountered from launch plus 70 s to launch plus 400 s, and assured that the samples

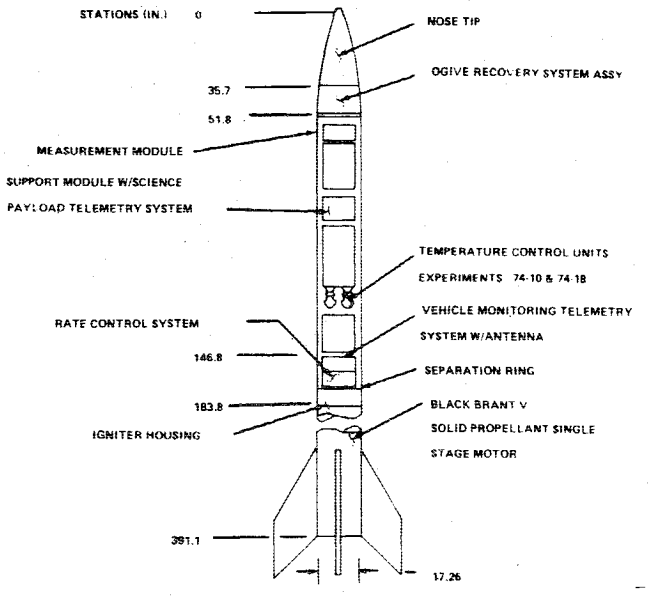

Fig. 4 Black Brant rocket with space processing payload (SPAR I).

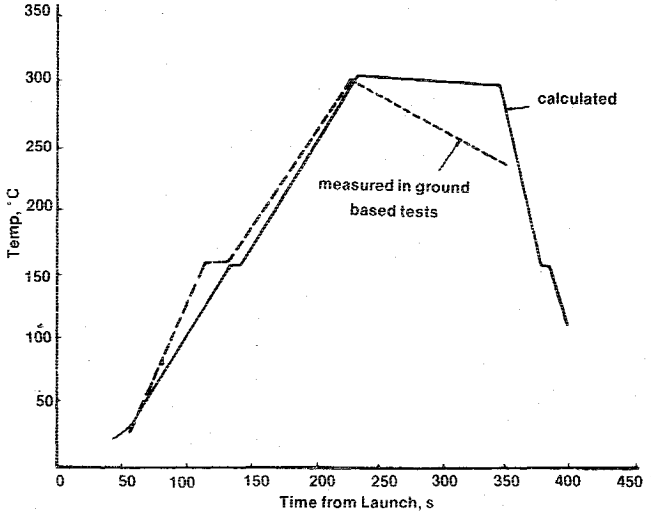

Fig. 5 Sample thermal history.

used in this experiment would be molten only during that low-g period. A temperature-vs-time profile for the sample is shown in Fig. 5.

III. Sample Characterization

An integrated record of fluid motions in the In-Pb samples during the low-g phase of the rocket trajectory was preserved in the resolidified samples. The x-ray absorption coefficients of the pure indium and the indium-lead alloy are sufficiently different that x-ray radiography with subsequent image analysis may be used to characterize this record of fluid motion. The processed samples were removed from the aluminum cartridges and inserted in an indium block placed on x-ray film as shown in Fig. 6. (The purpose of the indium block was to reduce effects of sample geometry on the resultant radiographs.) Exposures were made of each sample from multiple angles (sample rotated by 1/16 turn for each exposure) so that a three-dimensional record of the sample was preserved. After completing these exposures, 1-mm thick circular sections were taken from sample portions of particular interest and subjected to further x-ray radiography, the x-rays in this case being incident parallel to the sample

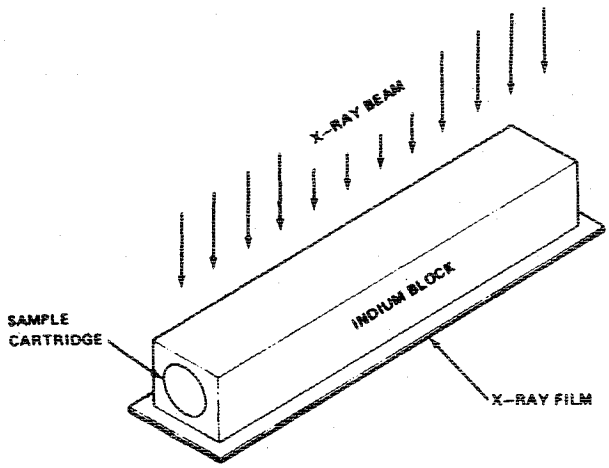

Fig. 6 X-ray radiography of samples.

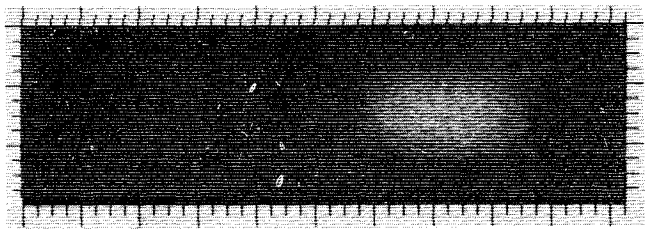

Fig. 7 Sample 1. Lighter material in In-Pb. Small graduations are approximately 0.5 mm. Radiograph through cylindrical sample.

cylinder axis. The x-ray radiographs were subjected to image analysis on the Marshall Space Flight Center Image Data Processing System (IDAPS). This system provides image enhancement capabilities and quantitative measurements of film relative gray scale values.

IV. Experimental Results

Thermal data telemetered from the flight samples indicated that the experiment performed as expected. Data from the three-axis accelerometer system and from the rate gyro system did not present a clear and consistent picture of the acceleration environment of the sounding rocket payload. The accelerometer data indicate acceleration levels as much as two orders of magnitude higher than those indicated by the data from the rate control system. In addition, the rate gyro data are not consistent with a torque-free system. A study at the Marshall Space Flight Center which brings some consistency to these data assumes offset bias in the accelerometer and/or the rate gyro data and assumes that a constant torque was applied to the payload.[7] These results indicate that a force (due to payload motion) was directed radially from the longitudinal axis of the payload and had a magnitude of approximately 10^{-6} g at the location of this experiment. Other components (perpendicular to the radial component) were down about an order of magnitude at that position according to these results.

Examination of the shape of the returned samples indicated that the samples had indeed melted and resolidified. The samples had rounded ends, and a small amount of shrinkage was evident along the sides of the samples. Radiographs of the returned samples were made to reveal any motion of the fluid system. Figures 7-9 are radiographs of the three cylindrical samples exposed with the x-ray beam perpendicular to the cylinder axis. The lighter portion of each radiograph represents the more dense In-Pb alloy, whereas the In is represented by the darker areas (which do not contrast well with the backgrounds). Radiographs of samples 1 and 2 reveal that the relative locations of the In and the In-Pb alloy were nearly unchanged during processing. That is, no convective

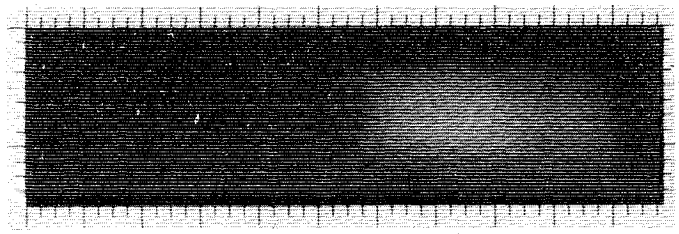

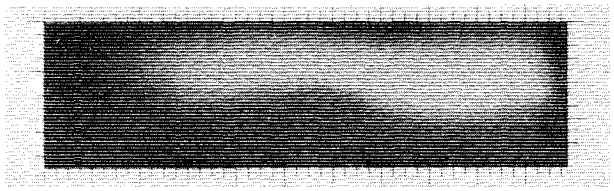

Fig. 9 Sample 3 (radiograph through cylindrical sample).

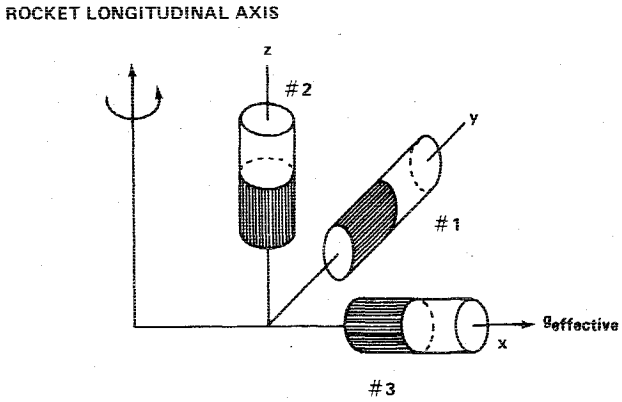

Fig. 10 Experiment configuration. Heavier material (In-Pb) shaded.

flow effects are evident. These samples were oriented relative to the payload as shown in Fig. 10. They were both perpendicular to a radius from the payload longitudinal axis and were, therefore, perpendicular to the major component of acceleration. Sample 3, which is nearly parallel to the major acceleration component and has the heavier material "up" with respect to that component, shows fluid motion on a scale comparable to the sample size. Figures 11 and 12 are radiographs of cross sections of sample 3, which further reveal the nature of the flow. Figure 11 represents a section 1 mm from the end of the sample that was originally pure In, and Fig. 12 represents a section near the middle of the sample. It is clear that flow took place in a nearly antisymmetrical manner along the sides of the sample. Figure 13 shows these results schematically.

V. Interpretation of Results

The results of the study of SPAR I payload motion cited earlier imply that the acceleration experienced by the liquid mixing experiment could to a close approximation be represented by a vector of fixed direction with respect to the experiment and of constant magnitude (approximately 10^{-6} g). The fluid behavior observed in the In-(In-Pb) samples is qualitatively consistent with a radial force of this nature. The arguments presented hereinafter attempt to place this correlation on a semiquantitative basis (semiquantitative in the sense that full time-dependent solutions to the fluid dynamical equations of motion are not found).

Samples 1 and 2

Samples 1 and 2 present the same aspect to the radial acceleration component, which we will label g-effective (g_{eff});

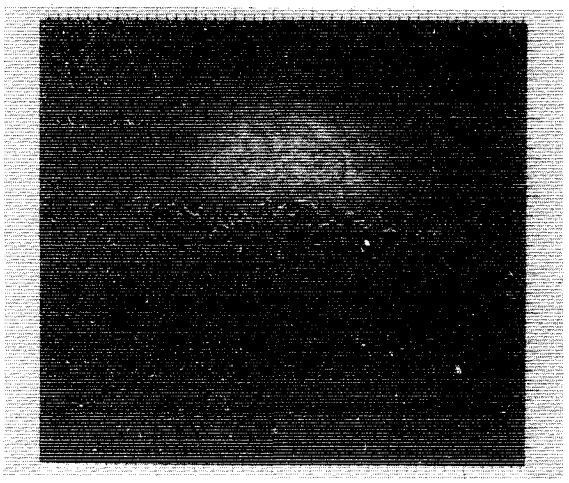

Fig. 11 Sample 3 (radiograph of 1-mm thick slice taken near end). White dots are from image analysis technique to define point of maximum film density change.

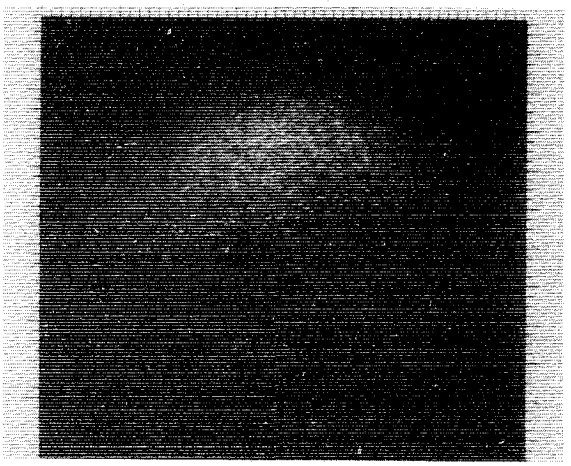

Fig. 12 Sample 3 (radiograph of 1-mm thick slice near center of sample.

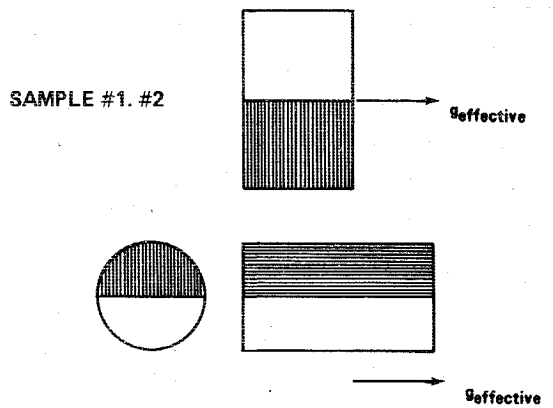

Fig. 13 Schematic of experimental results. Heavier material shaded.

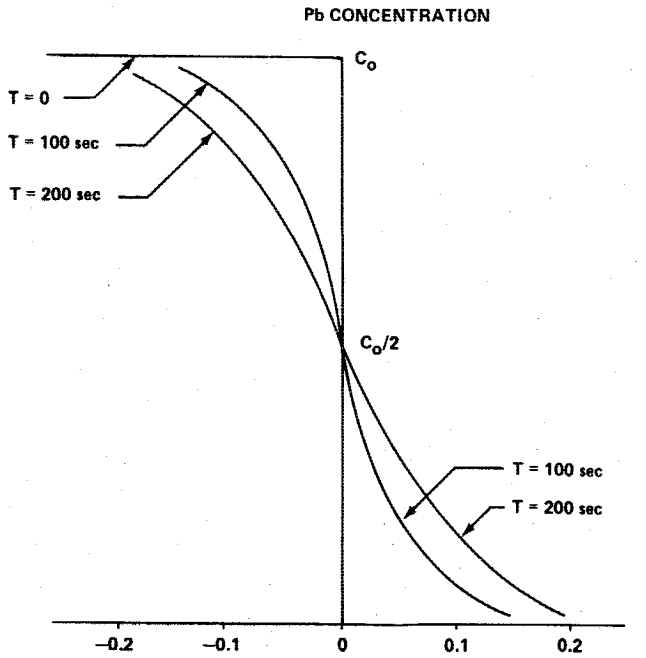

Fig. 14 Diffusion front motion (calculated).

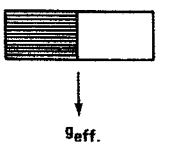

Fig. 15 Model for describing samples 1 and 2.

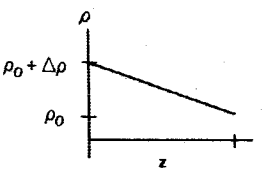

that is, the interface between the two materials is parallel to g_{eff}. The radiographs show that mixing in these samples was limited to a region about the thickness of the diffusion region; that is, within 1 mm of the original interface (see Fig. 14 for calculated diffusion front movement). The solution of this exact problem is not, to our knowledge, available. If we approximate our system with a two-dimensional rectangular system containing a linear density gradient (see Fig. 15) perpendicular to a hydrostatic pressure gradient, however, we may apply the nonlinear analysis of Cormack et al.[8] Using this model, we may calculate flow velocities in the neighborhood of the original interface and parallel to the sample container as a function of g_{eff}. Since fluid displacements in these samples were not greater than the width of the diffusion layer, we assume 0.2 cm of flow, which places an upper bound on g_{eff} of approximately 2×10^{-5} g. Figure 16 shows calculated interface motion as a function of g_{eff}. It was noted that the model assumes a linear density gradient rather than the step function gradient which exists in the sample. This results in the model producing an underestimation of the flow velocities for a given g_{eff}, thus overestimating the upper bound on g_{eff}. Both sample interfaces were deformed slightly within the diffusion width, which indicates that the estimate for the upper bound on g_{eff} given by this model should be on the order of 10^{-5} g.

Sample 3—Linear Theory

Some insight into the behavior observed in sample 3 may be gained through the application of Rayleigh-Taylor instability theory.[9] The sample is a stratified fluid with cylindrical geometry having the heavier material lying "above" the lighter material with respect to g_{eff} (see Fig. 10). Let us first discuss the role of surface tension. The application of Rayleigh-Taylor theory here involves writing the linear and, for simplicity, the inviscid Boussinesq equations in cylindrical coordinates for perturbations to an equilibrium state.

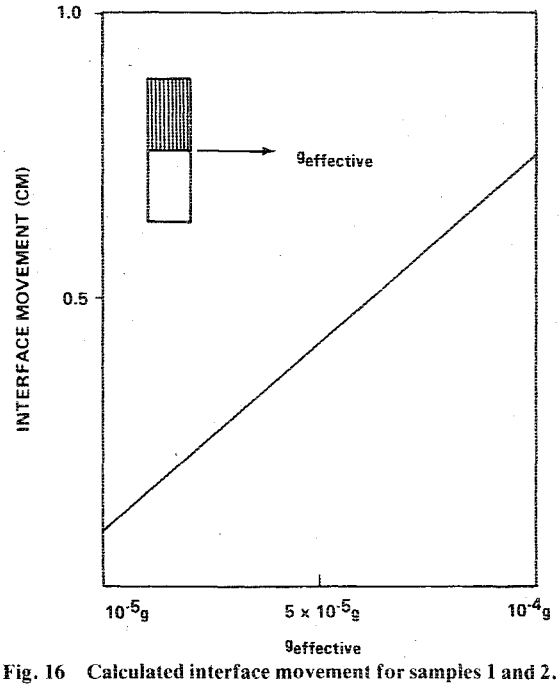

Fig. 16 Calculated interface movement for samples 1 and 2.

Solutions for the velocity perturbation are found to have the form

$$u = e^{\sigma_m t} J_m(\alpha_m r/a) e^{im\theta} F(z) \tag{1}$$

where r, θ, z are the cylindrical coordinates, t is time, σ_m is a perturbation growth rate parameter, a is the sample radius, and α_m is the disturbance wave number. Further analysis involving application of boundary conditions yields the following dispersion relation for the perturbation growth rate:

$$\sigma_m = \pm \alpha_m \sqrt{\frac{g_{\text{eff}}}{a}\left[\frac{(\Delta\rho/\rho) - (\alpha_m{}^2 T/a^2 g_{\text{eff}}\rho)}{(2-\Delta\rho/\rho)\coth\alpha_m h}\right]^{1/2}} \tag{2}$$

where $\Delta\rho$ is the difference in densities between the two materials, ρ is the density of the heavier material, T is the interface surface tension, and $2h$ is the cylinder height. It should be noted that Eq. (2) yields quantized growth rates; i.e., $m = 0,1,2,\ldots$. This quantization of the eigenstates is a result of the constraining cylindrical boundaries of the container. Quantized eigenstates should also occur in the viscous case. The nature of the behavior of this system may be illuminated by the preceding dispersion relation. We can see that for any finite value of surface tension (T) the expression in the braces will become negative for g_{eff} sufficiently small. This implies $\sigma_m = \pm iw$, and $u = A\ (r,\theta,z)\ e^{\pm iwt}$, which describe capillary waves at the interface. That is, no convective flow would occur, just oscillations of the interface. A similar result holds for the visous case. In the material system used for our samples, the two layers are miscible, so that surface tension should not persist at the interface ($T \to 0$). With σ_m real, we have the case in which the system is unstable to any perturbation, the perturbation growing without bound at the rate σ_m.

It should be noted that Eq. (2) predicts that the mode of maximum response occurs in the limit of infinitely long wave number α_m (i.e., vanishingly small disturbance size). Actually, viscosity suppresses the Rayleigh-Taylor instability at sufficiently large wave numbers, so that the mode of maximum response occurs at a finite, nonzero wave number. The Rayleigh-Taylor instability theory for a finite cylinder is not available. However, the results of the viscous theory for an unbounded fluid as given on p. 446 of Chandrasekhar[9] can

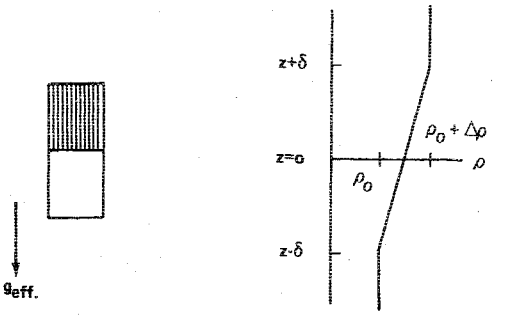

Fig. 17 Sample 3 model for predicted final state density gradient.

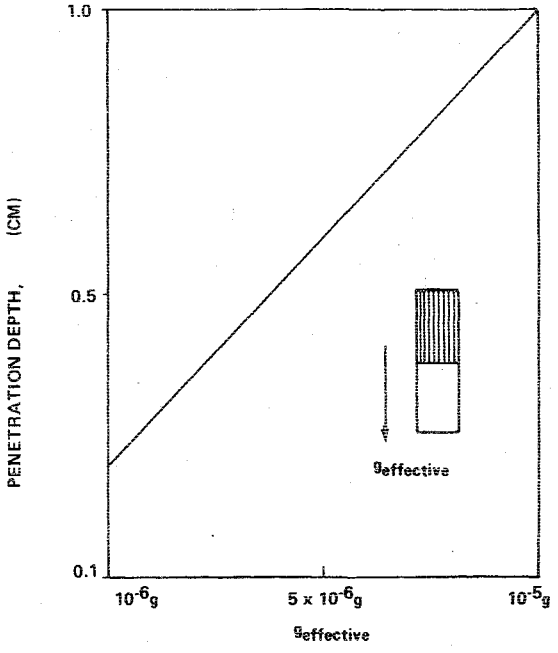

Fig. 18 Sample 3 predicted penetration depth as a function of gravity (effective).

be used to estimate growth rates. In the unbounded case the growth rate is a continuous function of wave number, while in our case the growth rates are discrete eigenvalues. Thus, to use the Chandrasekhar results, an estimate of the parameter α_m is required. We shall use the permissible disturbance wave number estimate from inviscid theory (this problem has a solution) and then apply these results to the unbounded viscous case. It is our opinion that reasonable order-of-magnitude estimates of the growth rate should be obtained with this procedure. Application of the viscous theory shows that the most unstable mode corresponds to $m = 1$, with $\alpha_1 = 1.84$. This mode corresponds to an antisymmetric motion relative to a plane containing the cylinder axis. This is just the type of motion observed in sample 3! The e-fold development times (σ_1^{-1}), which correspond to $m = 1$ for $g_{\text{eff}} = 10^{-6}$ and 10^{-5} g, were found to be 300 s and 50 s, respectively. Since the total experiment time is 200 s, the e-fold time for $g_{\text{eff}} = 10^{-6}$ appears too low, with that for $g_{\text{eff}} = 10^{-5}$ being consistent.

Sample 3—Nonlinear Effects

The previous discussion describes the behavior of a fluid system which models sample 3 for the onset of convective flow. After flow has begun, nonlinear effects become important. The nonlinear problem has not been worked, but insights to the behavior of the system may be gained from other experimental evidence and from dimensional analysis. Fluids systems very similar to sample 3 have been studied in a

1-g environment by Taylor[10] and by Wooding.[11] These experiments required much smaller tube diameter and smaller concentration gradients to be done in 1-g but should model the behavior of sample 3. It was observed that for a denser fluid overlaying a lighter fluid in a tube, the initial flow pattern was antisymmetric about a plane in which the cylinder axis lay. After a period of time, a final rest state of the fluid was reached. Here the heavier material still lay above the lighter, but the regions were connected by a region containing a linear density gradient (see Fig. 17). This final state is just the state defined by the critical Rayleigh number for a linear density gradient in an infinite cylinder (essentially the same results were obtained by Verhoeven[12] for a finite cylinder):

$$Ra = g_{\text{eff}}(\Delta\rho a^4/2\rho\delta\nu D) = 67.94$$

where Ra is Rayleigh number, δ is the penetration depth of heavier material into lighter material, ν is the kinematic viscosity, and D is the diffusivity. Results of penetration depth as a function of g_{eff} for this fluid system are shown in Fig. 18. For a penetration depth of 1 cm, we see that the value of g_{eff} required is approximately 10^{-5} g. This value is consistent with the development time scale calculation from the linear theory.

The state we observed in sample 3 was not the final state as described by Taylor and Wooding because radial density variations still exist. It was observed by those investigators, however, that the bulk of the convective motion occurred rapidly on the scale of time of the experiment, with diffusive mixing acting to bring about the final state. Mass diffusion and shear stresses induced by velocity gradients are the physical mechanisms whereby the convective motion eventually stops. If expected fluid velocities are such that flow distances on the order of the Taylor-Wooding penetration depth can be expected on the order of the time required for the diffusion time over the sample diameter, then the approach we have taken should give reasonable results. Following dimensional analysis arguments (e.g., Ostrach[13]), one obtains expected flow velocities on the order of 10^{-2} cm/s, which for the experiment time of 200 s represents the sample length. Taylor's formula[13] for the time required to remove density gradients in a tube

$$t = a^2/14.4D \approx 300 \text{ s}$$

gives a time on the order of the experiment time. This approach should then be valid.

VI. Summary and Conclusions

The results of this experiment show that buoyancy convection can occur even at very low effective gravity levels. We have seen that order-of-magnitude estimates of these flow effects can be made as a function of effective gravitational levels without being required to solve the fluid dynamical equations of motion (which will often not be possible). It is implicit also from these results that judicious experiment planning in the orientation and location of a fluids experiment in a payload can aid in reducing the effects of residual accelerations. We have also demonstrated that phenomenological studies in fluid dynamics relative to space processing can be performed on the SPAR which are not possible in a 1-g environment.

References

[1] *Proceedings Third Space Processing Symposium—Skylab Results*, Vol. I and II, Huntsville, Ala., April 30-May 1, 1974.

[2] "Apollo-Soyuz Test Project Preliminary Science Report," NASA TM X-58173, Feb. 1976.

[3] Bannister, T. C. and Grodzka, P. G., "Heat Flow and Convection Demonstration Experiments Aboard Apollo 14 and Apollo 17," *XXIV Congress of the International Astronautical Federation*, Baku, U.S.S.R., Oct. 1973.

[4] Bannister, T. C., "Postflight Analysis of Science Demonstrations," *AIAA/AGU Conference on Scientific Experiments on Skylab*, Huntsville, Ala., Oct. 30-Nov. 1, 1974.

[5] Ukanwa, A. O., "M558 Radioactive Tracer Diffusion," *Proceedings Third Space Processing Symposium—Skylab Results*, Vol. I, Huntsville, Ala., April 30-May 1, 1974.

[6] Hansen, M., *Constitution of Binary Alloys*, McGraw-Hill, New York, 1958, p. 854.

[7] Holland, R. L., "Acceleration Levels for Space Processing Application Rockets (SPAR)," NASA TM X-73351, 1976.

[8] Cormack, D. E., Leal, L. G., and Imberger, J., "Natural Convection in a Shallow Cavity with Differentially Heated End Walls. Part 1. Asymptotic Theory," *Journal of Fluid Mechanics*, Vol. 65, Pt. 2, 1974, pp. 209-229.

[9] Chandrasekhar, S., *Hydrodynamic and Hydromagnetic Stability*, Oxford University Press, London, 1961, pp. 428-477.

[10] Taylor, G. I., "Diffusion and Mass Transport in Tubes," *Proceedings of the Physical Society LXVII*, Vol. 12-B, 1955.

[11] Wooding, R. A., "The Stability of a Viscous Liquid in a Vertical Tube Containing Porous Material," *Proceedings of the Royal Society A.*, Vol. 252, 1969.

[12] Verhoeven, J. D., "Convection Effects in the Capillary Reservoir Technique for Measuring Liquid Metal Diffusion Coefficients," *Transactions of the Metals Society of AIME*, Vol. 242, Sept. 1968.

[13] Ostrach, S., "Convection Phenomena at Reduced Gravity of Importance for Materials Processing," Case Western Reserve University, NASA CR NAS8-31802, undated.